

Orbitally relieved magnetic frustration in NaVO₂

Ting Jia, Guoren Zhang and Zhi Zeng*

*Key Laboratory of Materials Physics, Institute of Solid State Physics,
Chinese Academy of Sciences, Hefei 230031, P. R. China*

H. Q. Lin

*Department of Physics and Institute of Theoretical Physics,
The Chinese University of Hong Kong, Shatin, Hong Kong, P. R. China*

(Dated: April 15, 2019)

The magnetic properties of NaVO₂ are investigated using full-potential linearized augmented plane wave method. We perform calculations for three structures. For the rhombohedral structure at 100 K, the t_{2g} orbitals of V ions are split into upper a_{1g} and lower e'_g orbitals by a trigonal distortion of compression. For the monoclinic structure at 91.5 K, the system behaves like a frustrated spin lattice with spatially anisotropic exchange interactions. For another monoclinic structure at 20 K, the magnetic frustration is relieved by a lattice distortion which is driven by a certain orbital ordering, and the long-range magnetic ordering is thus formed. Moreover, the small magnetic moment originates from the compensation of orbital moment for the spin moment.

* Correspondence author: zzeng@theory.issp.ac.cn

I. INTRODUCTION

The compounds with a common chemical formula ATO_2 ($A=\text{Na}$ or Li , $T=3d$ transition metals) have been attracting a lot of attention for their large variety and richness in physical phenomena[1, 2, 3, 4, 5, 6]. Indeed, the discovery of superconductivity in the $\text{Na}_{0.35}\text{CoO}_2 \cdot 1.3\text{H}_2\text{O}$ [1] and the application of LiCoO_2 in rechargeable Li batteries have accelerated investigations on their fundamental physics. In addition, NaMnO_2 undergoes a structural phase transition at 45 K to a long-range ordered antiferromagnetic (AFM) ground state[2], while NaNiO_2 exhibits ferromagnetic (FM) coupling in Ni-Ni plane below transition temperature[3]. Furthermore, a well-known member of this group, LiNiO_2 , has no long-range magnetic ordering even at low temperatures[4, 7, 8, 9]. The orbital frustration has been used to explain the absence of magnetic ordering[4, 7, 8], and a local ordering of Ni^{3+} Jahn-Teller (J-T) orbitals is also proposed to be responsible for the complex magnetic properties[9]. Therefore, its controversial magnetic properties have been attracting considerable interest.

These various phenomena always relate to the quasi-two-dimensional (2D) triangular lattice formed by T cations. Such a triangular lattice may lead to magnetic frustration, since all nearest-neighbor AFM interactions can not be satisfied simultaneously[2, 5, 6]. Nevertheless, the magnetic frustration can be relieved by a certain orbital ordering (OO)[10, 11, 12], such as in LiVO_2 [13] and NaVO_2 [14]. LiVO_2 has been found to form a spin-singlet phase with corresponding OO at low temperatures[5, 13]. Whereas, its sister compound NaVO_2 displays very different behaviours.

Recently, Onoda *et al.*[15] have revealed a superparamagnetic state driven by the short-range ordered spin-1 (the total spin in one trimer $S=1$) trimerization[16] below the transition temperature ($T=98$ K). However, McQueen *et al.* have reported two successive OO transitions in NaVO_2 [14]. At 98 K, the system undergoes a continuous phase transition from a rhombohedral ($R\bar{3}m$) phase to a monoclinic ($C2/m$) one, corresponding to the proposed OO of one electron per V^{3+} . Below 93 K, the system undergoes a discontinuous phase transition to another monoclinic ($C2/m$) phase, consistent with the proposed OO of two electron per V^{3+} . In addition, a long-range ordered AFM state is formed at low temperatures, while the magnetic moment observed in the ordered phase is about $0.98 \mu_B$, much smaller than the expected value ($2 \mu_B$). The controversial magnetic states below 98 K obtained by these two groups bring us interests, and the puzzling magnetic moment deserves to be explored. There are no theoretical reports yet to the best of our knowledge, therefore we expect to understand its magnetic properties at low temperatures upon our theoretical efforts.

In the present work, we have performed first-principles calculations to investigate the electronic structures of NaVO₂, further to reveal the most possible orbital and magnetic ordering, and to explore the origin of small magnetic moment observed at low temperatures. Partially in agreement with the experimental findings[14], the OO, accompanied by a long-range magnetic ordering, is found for the second monoclinic structure. And the observed magnetic moment can be explained by including the spin-orbit coupling (SOC) interactions.

This paper is organized as follows. The crystal structure and computational details are described briefly in Sec. II. And the results and discussions are presented in Sec. III. Finally, a brief conclusion is summarized in Sec. IV.

II. CRYSTAL STRUCTURE AND COMPUTATIONAL DETAILS

The lattice parameters provided by McQueen *et al.* are listed in Table I. The structure of NaVO₂ is composed of 2D triangular-lattice VO₂ layers of edge sharing VO₆ octahedra separated by sodium ions, which is rhombohedral ($R-3m$) at relatively high temperature (HT) ($T > 98$ K) and monoclinic ($C2/m$) in both intermediate temperature (IT) ($91.5 \text{ K} < T < 98 \text{ K}$) and low temperature (LT) ($T < 91.5 \text{ K}$) phases[14]. At 100 K, the V-O distances are nearly 2.04 Å, but the O-V-O angle α is only 85.53° (Fig. 1). With lowering the temperature, α further reduces to 85.42° at 91.5 K and 85.13° at 20 K. Therefore, even in the HT phase, VO₆ octahedra in NaVO₂ have been different from the regular ones under a trigonal distortion of compression along the threefold (111) axis[14], which induces the lowering of the O_h local symmetry to D_{3d} . In VO₂ layers, the V-V geometry is built by two long (3.00781 Å) and four short (2.99316 Å) bonds in the IT phase, and reversely is by two short (2.97551 Å) and four long (3.00526 Å) ones in the LT phase[17]. The interlayer V-V distance is about 5.6 Å.

All the calculations were performed by using the standard full-potential linearized augmented plane wave code WIEN2k[18]. The muffin-tin sphere radii of 2.22, 2.00 and 1.77 a.u. were chosen for the Na, V and O atoms, respectively. The cutoff parameter $R_{mt}K_{max}$ was chosen to be 7.0 and 100 k -points were used over the first Brillouin zone. The local spin density approximation (LSDA) of Perdew and Wang[19] was used for the exchange and correlation potential. In order to take the strong-correlated nature of 3d electrons into account explicitly, we performed LSDA+U calculations[20], where $U_{eff}=U-J$ (U and J are on-site Coulomb and exchange interaction respectively) was used instead of U [21]. And the orbital-dependent potential has the form of ΔV_{FLL}

$= -U_{eff}(\hat{n}^\sigma - \frac{1}{2}I)$ [22], where \hat{n}^σ is the orbital occupation matrix of spin σ . This type of double-counting correction (DCC) has been called the fully localized limit[23] and demonstrated better agreement with experiment than other DCC[24]. For NaVO_2 , we used $U_{eff}=3.6$ eV which has been used in its sister compound LiVO_2 [5]. Note also that the conclusion made in this paper is not affected for $U_{eff}=2-6$ eV[25]. To explore the origin of small magnetic moment observed in the LT phase, we performed LSDA+SOC+U calculations, where the SOC is included by the second-variational method with scalar relativistic wave functions[18]. The easy magnetization direction was set along $(\bar{1}10)$ direction (short V-V bonds in the LT phase) observed in the experiment[14].

In order to investigate different magnetic patterns, $2 \times 2 \times 2$ supercell was used in our calculations. We took into account two AFM structures in V-V plane as described in Fig. 2(a): I-type antiferromagnetism (Fig. 2(a)(i)) is AFM exchange along the (010) and $(\bar{1}10)$ directions with FM exchange along the (100) direction, II-type antiferromagnetism (Fig. 2(a)(ii)) is AFM exchange along the (100) and (010) directions with FM exchange along the $(\bar{1}10)$ direction. Totally there were five possible magnetic configurations in our calculations for the IT and LT phases (Fig. 2(b)): ferromagnetic (FM), C-AFI (I-type antiferromagnetism in plane, FM stacking), C-AFII (II-type antiferromagnetism in plane, FM stacking), G-AFI (I-type antiferromagnetism in plane, AFM stacking), G-AFII (II-type antiferromagnetism in plane, AFM stacking).

III. RESULTS AND DISCUSSIONS

A. HT phase

As the paramagnetic behavior of NaVO_2 has been determined from the magnetic susceptibility measurements in the HT phase[14, 15], we just focus on the electronic structure instead of its magnetic properties.

The band structures obtained from LSDA and LSDA+U calculations are shown in Fig. 3. Within LSDA (Fig. 3(a)), the bands near the Fermi level (E_F) are mainly derived from V $3d$ states. Since straight V-O-V paths are not present in layered NaVO_2 and instead only nearly 90° V-O-V bonds exist, the V $3d$ states are quite narrow. In the approximately octahedral crystal field, the $3d$ orbitals are split into upper e_g and lower t_{2g} states. As shown in Fig. 3(a), e_g derived bands range from 1.5 to 2.5 eV and t_{2g} derived bands lie between -1.5 and 0.5 eV. The splitting between t_{2g} and e_g bands is about 1 eV. Under the trigonal crystal field, the t_{2g} orbitals are further split into

one a_{1g} and two degenerate e'_g orbitals. However, the splitting is much less than the band widths so that the t_{2g} orbitals still cross the E_F , which denotes a metallic state within LSDA. That is to say, LSDA calculations can not reproduce the insulating nature of NaVO_2 from experiment[14]. The LSDA+U scheme[20] is thus used to count the strong correlation of V 3d electrons. As shown in Fig. 3(b), the empty a_{1g} band is pushed upwards by about 1 eV, and a gap is opened near the E_F . The system is hence an insulator due to electron correlation and NaVO_2 is indeed a good candidate for Mott-Hubbard insulator.

According to the pure crystal field theory, the a_{1g} orbital is of lower energy than the e'_g orbitals under the trigonal distortion of compression, which is opposite to our LSDA+U results. So it is necessary to discuss the controversy on relative order of a_{1g} - e'_g in such trigonal distortions. In Ref. [26], Landron and Lepetit pointed out that this relative order is strongly influenced by the e_g - e'_g hybridization. The e_g and e'_g orbitals belong to the same irreducible representation (E_g) and can thus mix despite the large t_{2g} - e_g energy difference. Such a mix may be small but it modulates large energetic factors: the on-site Coulomb repulsions. When the e_g - e'_g hybridization is taken into account, the energy difference ΔE between the a_{1g} and e'_g orbitals depends on two competitive parts: $\Delta E = \Delta E_1 + \Delta E_2 = \varepsilon(a_{1g}) - \varepsilon(e'_g)$. ΔE_1 includes the kinetic energy, the electron-charge interaction, and the interaction with the core electrons. ΔE_2 denotes the repulsion and exchange terms within the 3d shells. Additionally, ΔE_1 and ΔE_2 both depend on the amplitude of the trigonal distortion and are of opposite effect with each other. Under a trigonal distortion of compression, if we only consider the crystal field effect (ΔE_1), the a_{1g} orbital is of lower energy than the e'_g orbitals ($\Delta E < 0$). Whereas if we take ΔE_2 into account, the relative order between the a_{1g} and e'_g orbital is reversed ($\Delta E > 0$), comparing with the crystal field prediction. Therefore, LSDA+U calculations predict that the a_{1g} orbital is of higher energy than the e'_g orbitals in NaVO_2 . In fact, such a controversy has been presented in another compressed triangular system Na_xCoO_2 [27, 28, 29]. From the crystal field theory, some authors[27] proposed that the energy of a_{1g} orbital is lower than the e'_g orbitals. However, the LDA+U method[28, 29] yielded an a_{1g} orbital of higher energy than the e'_g orbitals. Later, the experimental results[30] showed that the Fermi surface of the CoO_2 layers issues from the a_{1g} orbital, not at all from the e'_g orbitals, supporting the LDA+U results.

B. IT phase

The triangular lattice of NaVO₂ exhibits magnetic frustration and spatially anisotropic exchange interactions in the IT phase. As shown in Table II, the *G*-AFI configuration is the most stable state among the five magnetic structures both from LSDA and LSDA+U calculations. By a detailed analysis of the magnetic ground state *G*-AFI, see Fig. 2(a)(i), AFM chains are formed along the ($\bar{1}10$) direction (long V-V bonds), while AFM exchange is also more favorable along the (010) direction (short V-V bonds). Considering all the short V-V bonds are completely equivalent, both of the (100) and (010) directions should be AFM exchange. Thus, NaVO₂ in the IT phase can be regarded as a system with frustration effects. In addition, spatially anisotropic exchange interactions may exist in such a triangular spin lattice[2], i.e., J_1 along the direction of long V-V bonds and J_2 along the two directions of short V-V bonds (Fig. 2(a)(i)).

In order to describe the magnetic frustration and spatially anisotropic exchange interaction more clearly, we estimate the exchange interactions along one of the triangle directions (J_1) and the other two (J_2) (Fig. 2(a)(i)). Since all the configurations exhibit insulator characteristics, the spin size of V is stable, and the difference of total energy between *C*-AFI and *G*-AFI (*C*-AFII and *G*-AFII) configurations (See Table II) is so small that the system exhibits a 2D characteristic, a nearest neighbor Heisenberg-like Hamiltonian may be a good primary approximation for the in-layer magnetic energy. The corresponding 2D spin Hamiltonian can be written as

$$H = J_1 \sum_{(k,l)} \mathbf{S}_k \cdot \mathbf{S}_l + J_2 \sum_{(i,j)} \mathbf{S}_i \cdot \mathbf{S}_j \quad (1)$$

where (i,j) denotes a nearest-neighbor pair (short V-V bond) and (k,l) denotes a next-nearest-neighbor pair (long V-V bond). By mapping the obtained total energies for each magnetic state to the Heisenberg model, the exchange interactions J_1 and J_2 were calculated within this approximation:

$$2 \times (8 \times 4J_2S^2) = E(FM) - E(C - AFII) \quad (2)$$

$$2 \times (4 \times 4J_2S^2 + 4 \times 4J_1S^2) = E(FM) - E(C - AFI) \quad (3)$$

With $S=1$, we get $J_2=2.1$ meV and $J_1=6.1$ meV for NaVO₂ in the IT phase, which reflects strong spatial anisotropy. The AFM chains are established along the ($\bar{1}10$) direction (J_1) and the inter-chain coupling (J_2) is frustrated. Moreover, the value of $J_2/J_1=0.3$ is so small that this magnetic structure can be described as so-called weakly coupled *zigzag* ($S=1$) chains model[31].

The integer spins ($S=1$) are able to weaken the frustration effects in the frustrated systems, as in kagomé lattice[32]. Such a lattice has four nearest neighbors with the adjacent triangles on the lattice sharing only one lattice point. Interestingly, the triangular lattice can be composed of four kagomé lattices[27]. Thus, there are some analogous properties in these two frustrated systems. Therefore, it is reasonable to suppose that the triangular lattice also has the rule that the half-odd-integer spins are more highly frustrated than integer ones. For example, NaTiO_2 ($S = \frac{1}{2}$)[5] and LiCrO_2 ($S = \frac{3}{2}$)[6] with half-odd-integer spins are always frustrated even at low T , while the magnetic frustration of NaMnO_2 ($S=2$) is clearly lifted by a structural distortion[2]. Besides NaMnO_2 , NaVO_2 is another typical triangular lattice with integer spins ($S=1$). Therefore, we can presume that the magnetic frustration in NaVO_2 can be lifted in some way.

C. LT phase

From the discussion above, we expect that NaVO_2 with $S=1$ will show a long-range magnetic ordering or a finite ground-state magnetization at low T . As shown in Table II, G -AFII is only 0.3 meV lower in total energy than C -AFII within LSDA, and both G -AFII and C -AFII have the same lowest total energy from LSDA+U results for the LT phase. This reflects the obvious 2D characteristic of NaVO_2 : the interlayer interaction is much weaker than the intralayer one. As stacking antiferromagnetically between layers is observed in the experiment[14], G -AFII state should be more favorable at low T . Such a magnetic state denotes the long range 3D magnetic ordering with AF coupled FM chains in V cation layers and interlayer AF coupling. Obviously, the magnetic frustration is lifted in G -AFII state by the first-order transition at 91.5 K: the lattice distorts to another monoclinic ($C2/m$) with four long and two short V-V bonds reversed, comparing with IT phase.

The lattice distortion, which relieves the frustration, is driven by the formation of OO in the LT phase. Fig. 4 shows the orbital characteristic of V $3d$ in G -AFII state. Since the orbital occupancies of the two inequivalent V (V1 and V2 in Fig. 2(a)(ii)) are nearly the same, only the density of states (DOS) of V1 $3d$ is shown. The z axis of local coordinate system coincides with the V-O bond of the VO_6 octahedra. In such a coordinate system, d_{zx} and d_{yz} orbitals are mainly occupied and d_{xy} orbital is less occupied at all V ions. Such an orbital occupancy is consistent with the OO proposed by McQueen and Cava[14]: the d_{zx} and d_{yz} orbitals are singly occupied with all unoccupied d_{xy} orbitals.

This OO relieves the magnetic frustration and stabilizes the long-range magnetic ordering state. In view of the weak superexchange interaction resulted from the nearly 90° angle of V-O-V[33] as well as the weak magnetic interaction between adjacent VO_2 planes interleaved by a layer of Na ions, the V-V direct exchange interaction in-plane should be dominant in such a particular crystal structure. Particularly, we only consider the σ overlap in V-V direct exchange, which is much stronger than the π overlap. It means that each orbital in a V ion only hybridizes with the same orbitals in the two nearest-neighboring V ions. That is to say, d_{yz} orbital hybridizes with two neighboring d_{yz} orbitals in the (010) and (0 $\bar{1}$ 0) directions, and d_{zx} orbital hybridizes with two neighboring d_{zx} orbitals in the (100) and ($\bar{1}$ 00) directions. The repulsions between the occupied orbitals (d_{zx} or d_{yz}) induce the elongation of V-V bonds along four directions: (010), (0 $\bar{1}$ 0), (100) and ($\bar{1}$ 00). According to the Goodenough-Kanamori (GK) rules[34], the strong AFM coupling should exist along these four directions because of the occupation of two orbitals with σ overlap. At the same time, the less occupancy of d_{xy} orbital leads to V-V bonds contraction as well as a weak FM exchange along the (1 $\bar{1}$ 0) and ($\bar{1}$ 10) directions. Thus, the four long and two short V-V bonds result from bonding via d_{zx} , d_{yz} orbitals, but no bonding of the d_{xy} electrons. In other words, such an OO results in the lattice distortion, and consequently relieves the magnetic frustration.

In the LT phase, another important aspect is that the SOC turns out to be crucial for the small magnetic moment of $0.98 \mu_B$ per V^{3+} observed experimentally[14]. As shown in Table II, the magnetic moments from LSDA+U calculations are much larger than the ones observed in the experiment. Further to investigate the magnetic moments changing with the particular choice of U_{eff} , we calculate the moments for $U_{eff}=2-6$ eV and find that the moments are not sensitive to U_{eff} : as shown in Table III, the magnetic moments stay constant within $0.2 \mu_B$ as long as the system is an insulator. Since an easy magnetization direction ($\bar{1}$ 10) is observed in the experiment[14], the SOC may play an important role in determining the total magnetic moment. Thus, the SOC is included to reinvestigate the magnetic moment.

Then, we perform LSDA+SOC+U calculations for the favorable magnetic configuration (G -AFII), and obtain a local moment of $0.89 \mu_B$ per V^{3+} with $1.65 \mu_B$ spin and $-0.77 \mu_B$ orbital contributions. This value is half the expected moment ($2 \mu_B$), but very close to the observed one ($0.98 \mu_B$). The DOS projected on (2,m) space shown in Fig. 5 reveals the origin of orbital moment. Note that the z axis is set to the direction of easy magnetization along ($\bar{1}$ 10) now. Since d_1 and d_{-1} have nearly the same occupancies, the orbital moment only comes from the contribution of different occupancies between d_2 and d_{-2} . By further analysis, the d_2 occupancy is less than

one half of the d_{-2} one, which should give an orbital moment between $1 \mu_B$ and $2 \mu_B$. Nevertheless, there is no surprising that the calculated orbital moment is $0.77 \mu_B$ here, because some hybridization effects are neglected in above analysis, e.g., the covalence effects with O $2p$. Thus, the inclusion of SOC leads to a surprising but experimentally sound results.

IV. CONCLUSIONS

Summarizing, we have investigated the electronic structure and magnetic properties of NaVO_2 by first-principles calculations. The t_{2g} orbitals are split into upper a_{1g} and lower e'_g states by a trigonal distortion of compression in the HT phase, which is similar to the splitting in Na_xCoO_2 [28]. In the IT phase, the crystal symmetry is lowered to $C2/m$, under which the system behaves like a frustrated spin lattice with spatially anisotropic exchange interactions. Finally, a certain ordering of occupied orbitals is formed at low T , resulting in another lattice distortion and relieving the magnetic frustration. And a long-range ordered AF ground state is thus formed. The small magnetic moment observed origins from the compensation of orbital moment for the spin moment. It is obvious that so many physics phenomena in the triangular lattice are reflected in NaVO_2 , suggesting that NaVO_2 is a very good model material for studying 2D triangular lattice systems.

V. ACKNOWLEDGEMENTS

We thank T. M. McQueen, P. W. Stephens, Q. Huang, T. Klimczuk, F. Ronning, and R. J. Cava for providing structural parameters prior to publication. This work was supported by the special Funds for Major State Basic Research Project of China(973), 863 Project, Knowledge Innovation Program of Chinese Academy of Sciences, and Director Grants of CASHIPS, CUHK Direct Grant No. 2160345. Part of the calculations were performed in Center for Computational Science of CASHIPS and the Shanghai Supercomputer Center.

-
- [1] K. Takada, H. Sakurai, E. Takayama-Muromachi, F. Izumi, R. A. Dilanian, and T. Sasali, Nature (London) **422**, 53 (2003).

- [2] Maud Giot, Laurent C. Chapon, John Androulakis, Mark A. Green, Paolo G. Radaelli, and Alexandros Lappas, *Phys. Rev. Lett.* **99**, 247211 (2007).
- [3] C. Darie, P. Bordet, S. de Brion, M. Holzapfel, O. Isnard, A. Lecchi, J. E. Lorenzo, and E. Suard, *Eur. Phys. J. B* **43**, 159 (2005).
- [4] F. Reynaud, D. Mertz, F. Celestini, J.-M. Debierre, A. M. Ghorayeb, P. Simon, A. Stepanov, J. Voiron, and C. Delmas, *Phys. Rev. Lett.* **86**, 3638 (2001).
- [5] S. Yu. Ezhov, V. I. Anisimov, H. F. Pen, D. I. Khomskii and G. A. Sawatzky, *Europhys. Lett.* **44**, 491 (1998).
- [6] I. I. Mazin, *Phys. Rev. B* **75**, 094407 (2007).
- [7] Albert J. W. Reitsma, Louis Felix Feiner and Andrzej M. Oleś, *New J. Phys.* **7**, 121 (2005).
- [8] F. Mila, F. Vernay, A. Ralko, F. Becca, P. Fazekas and K. Penc, *J. Phys.: Condens. Matter* **19**, 145201 (2007).
- [9] J.-H. Chung, Th. Proffen, S. Shamoto, A. M. Ghorayeb, L. Croguennec, W. Tian, B. C. Sales, R. Jin, D. Mandrus and T. Egami, *Phys. Rev. B* **71**, 064410 (2005).
- [10] Y. Tokura and N. Nagaosa, *science*, **288**, 462 (2000)
- [11] J.-Q. Yan, J.-S. Zhou, and J. B. Goodenough, *Phys. Rev. Lett.* **93**, 235901 (2004).
- [12] Peter Horsch, Andrzej M. Oleś, Louis Felix Feiner, and Giniyat Khaliullin, *Phys. Rev. Lett.* **100**, 167205(2008).
- [13] H. F. Pen, J. van den Brink, D. I. Khomskii, and G. A. Sawatzky, *Phys. Rev. Lett.* **78**, 1323 (1997).
- [14] T. M. McQueen, P. W. Stephens, Q. Huang, T. Klimczuk, F. Ronning, and R. J. Cava, *Phys. Rev. Lett.* **101**, 166402 (2008).
- [15] M. Onoda, *J. Phys. Condens. Matter* **20**, 145205 (2008).
- [16] H. F. Pen, L. H. Tjeng, E. Pellegrin, F. M. F. de Groot, G. A. Sawatzky, M. A. van Veenendaal and C. T. Chen, *Phys. Rev. B* **55**, 15500 (1997).
- [17] The difference between 93 K and 91.5 K has to do with the sample being measured on warming or on cooling. The IT to LT transition temperature is $T=91.5$ K here, corresponding to the lattice parameters measured on cooling. And the slight lattice-parameter differences from Ref. [14] are within experimental error.
- [18] P. Blaha *et al.*, <http://www.wien2k.at>.
- [19] John P. Perdew and Yue Wang, *Phys. Rev. B* **45**, 13244 (1992).
- [20] Vladimir I. Anisimov, Jan Zaanen, and Ole K. Andersen, *Phys. Rev. B* **44**, 943 (1991).

- [21] S. L. Dudarev, G. A. Botton, S. Y. Savrasov, C. J. Humphreys and A. P. Sutton, Phys. Rev. B **57**, 1505 (1998).
- [22] G. K. H. Madsen and P. Novak, Europhys. Lett. **69**, 777 (2005).
- [23] V. I. Anisimov, I. V. Solovyev, M. A. Korotin, M. T. Czyżyk and G. A. Sawatzky, Phys. Rev. B **48**, 16929 (1993).
- [24] Robert Laskowski, Peter Blaha, and Karlheinz Schwarz, Phys. Rev. B **67**, 075102 (2003).
- [25] We performed LSDA+U calculations for the two most stable configurations (*G*-AFI and *G*-AFII) both in the IT and LT phases with $U_{eff}=2, 3, 5, 6$ eV. The results show that the *G*-AFI (*G*-AFII) is always the most stable state in the IT (LT) phase in such U_{eff} range.
- [26] Sylvain Landron and Marie-Bernadette Lepetit, Phys. Rev. B **77**, 125106 (2008).
- [27] W. Koshibae and S. Maekawa, Phys. Rev. Lett. **91**, 257003 (2003).
- [28] Sylvain Landron and Marie-Bernadette Lepetit, Phys. Rev. B **74**, 184507 (2006).
- [29] Liang-Jian Zou, J.-L. Wang, and Z. Zeng, Phys. Rev. B **69**, 132505 (2004).
- [30] M. Z. Hasan, Y.-D. Chuang, D. Qian, Y. W. Li, Y. Kong, A. P. Kuprin, A.V. Fedorov, R. Kimmerling, E. Rotenberg, K. Rossnagel, Z. Hussain, H. Koh, N. S. Rogado, M. L. Foo, and R. J. Cava, Phys. Rev. Lett. **92**, 246402 (2004).
- [31] Zheng Weihong, Ross H. McKenzie and Rajiv R. P. Singh, Phys. Rev. B **59**, 14367 (1999).
- [32] Swapan K. Pati and C. N. R. Rao, J. Chem. Phys. **123**, 234703 (2005).
- [33] J. B. Goodenough, Phys. Rev. **117**, 1442 (1960).
- [34] J. B. Goodenough, *Magnetism and the Chemical Bond* (Interscience Publishers, New York, 1963); J. Kanamori, J. Phys. Chem. Solids **10**, 87 (1959).

TABLE I: The lattice parameters of NaVO₂ at 100, 91.5 and 20 K

Temperature	100 K	91.5 K	20 K
space group	<i>R-3m</i>	<i>C2/m</i>	<i>C2/m</i>
a(Å)	2.9959(1)	5.1758(1)	5.2223(2)
b(Å)	2.9959(1)	3.0078(1)	2.9755(1)
c(Å)	16.0996(1)	5.6340(1)	5.6492(3)
α (°)	90	90	90
β (°)	90	107.629(1)	108.335(1)
γ (°)	120	90	90
x,y,z(Na)	3a(0, 0, 0)	2a(0, 0, 0)	2a(0, 0, 0)
x,y,z(V)	3b(0, 0, 0.5)	2d(0, 0.5, 0.5)	2d(0, 0.5, 0.5)
x,y,z(O)	6c(0, 0, 0.2339(0))	4i(0.2368(7), 0, 0.6989(5))	4i(0.2296(5), 0, 0.7005(4))

TABLE II: The total energy E (meV/ (8f. u.)), magnetic moment M (μ_B) per V^{3+} and band gap E_g (eV) in different magnetic states.

		Configuration	FM	C-AFI	G-AFI	C-AFII	G-AFII
LSDA	IT (T=91.5 K)	E	37.8	0.3	0	9.4	9.7
		M	1.63	± 1.37	± 1.37	± 1.34	± 1.34
	LT (T=20 K)	E	42.2	11.2	11.5	0.3	0
		M	1.51	± 1.35	± 1.35	± 1.38	± 1.38
LSDA+U	IT (T=91.5 K)	E	24.2	4.8	0	14.1	13.9
		M	1.71	± 1.65	± 1.65	± 1.66	± 1.66
		E_g	1.1	1.2	1.1	1.4	1.5
	LT (T=20 K)	E	29.0	21.0	21.2	0	0
		M	1.71	± 1.66	± 1.66	± 1.65	± 1.65
		E_g	1.2	1.4	1.4	1.1	1.1

TABLE III: The band gap E_g (eV) and magnetic moment M (μ_B) per V^{3+} for different U_{eff} (eV) in G -AFII configuration.

U_{eff}	2	3	3.6	5	6
E_g	0.02	0.9	1.1	1.8	2.3
M	± 1.57	± 1.63	± 1.65	± 1.69	± 1.71

FIG. 1: (color online). (a) The compressed octahedron of VO_2 layers. The z axis is the three fold axis of the VO_6 octahedron. α represents the O-V-O angle. (b) α angles in the HT, IT and LT phases.

FIG. 2: (a) Two different magnetic patterns in V-V plane (i) I-type AF and (ii) II-type AF. The solid (dashed) lines represent short V-V bonds in the IT (LT) phase and dashed (solid) lines represent long V-V bonds in the IT (LT) phase. J_1 (J_2) denotes exchange interaction along the direction of dashed (solid) lines. (b) Schematic representation of five magnetic configurations used in our calculation. Only V atoms are drawn. Filled (open) circles indicate spin up (down) moments.

FIG. 3: The spin-majority band structure of NaVO_2 from (a) LSDA and (b) LSDA+U calculations for the fixed structure at 100 K. The band with (a) $3d$ and (b) a_{1g} character is marked.

FIG. 4: Density of states (DOS) of NaVO_2 calculated by LSDA+U in the G -AFII state for the fixed structure at 20 K. Besides total $3d$ state, all the d_{zx} , d_{yz} and d_{xy} orbitals in local coordinate system for V1 (Fig. 2(a)(i)) ion are depicted. Solid (dashed) lines denote the spin-up (down) states.

FIG. 5: Density of states (DOS) of NaVO_2 calculated by LSDA+U+SOC in the G -AFII state for the fixed structure at 20 K. Solid (dashed) lines denote the spin-up (down) states.

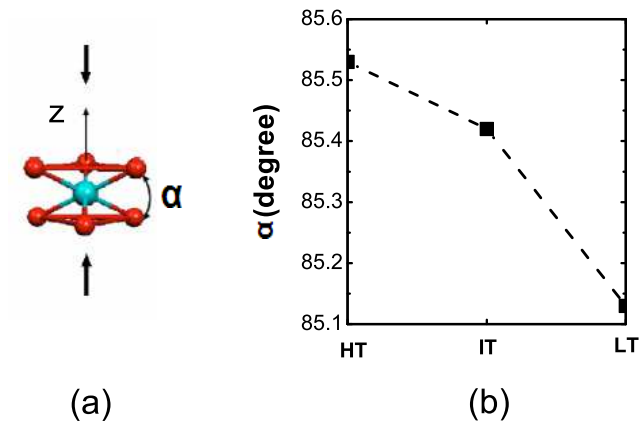
Fig. 1 tjia.eps

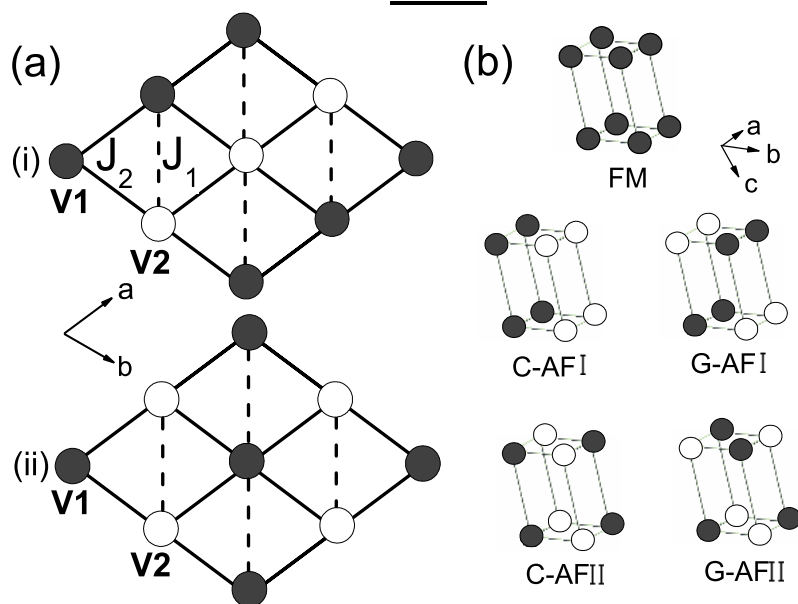
Fig. 2 tjia.eps

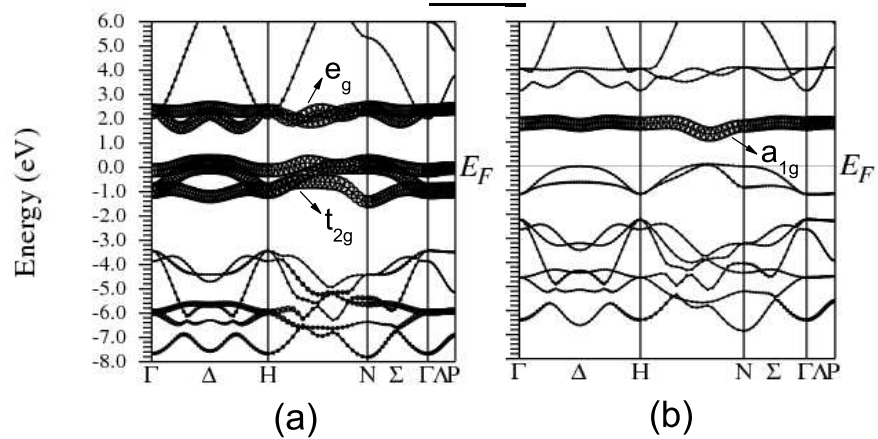
Fig. 3 tjia.eps

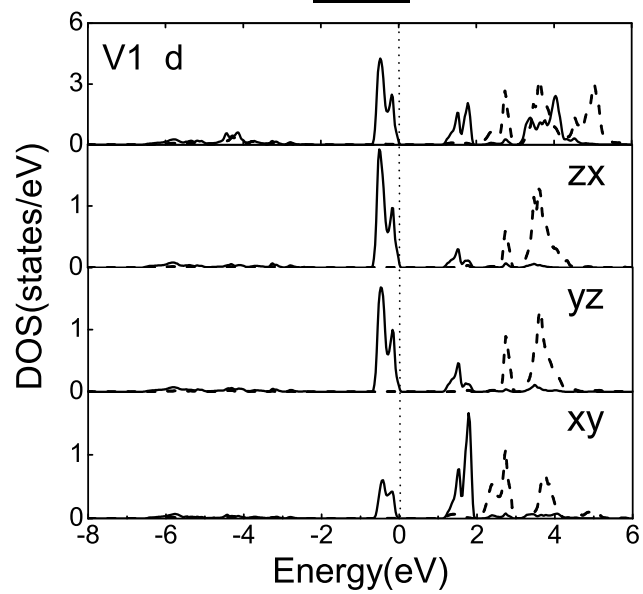
Fig. 4 tjia.eps

Fig. 5 tjia.eps